Numerical simulations of output pulse extraction from a high-power microwave compressor with a plasma switch

Anatoli Shlapakovski,[1] Leonid Beilin,[1] Yuri Bliokh,[1] Moshe Donskoy,[1] Yoav Hadas,[2] Edl Schamiloglu,[3] and Yakov E. Krasik[1]
[1]*Physics Department, Technion, Haifa 32000, Israel*
[2]*Department of Applied Physics, Rafael, PO Box 2250, Haifa 31021, Israel*
[3]*Department of Electrical and Computer Engineering, University of New Mexico, Albuquerque, New Mexico 87131, USA*

(Received 21 February 2014; accepted 25 April 2014; published online 7 May 2014)

Numerical simulations of the process of electromagnetic energy release from a high-power microwave pulse compressor comprising a gas-filled cavity and interference switch were carried out. A microwave plasma discharge in a rectangular waveguide H-plane tee was modeled with the use of the fully electromagnetic particle-in-cell code MAGIC. The gas ionization, plasma evolution, and interaction with RF fields accumulated within the compressor were simulated using different approaches provided by the MAGIC code: particle-in-cell approach accounting for electron-neutral collisions, gas conductivity model based on the concept of mobility, and hybrid modeling. The dependences of the microwave output pulse peak power and waveform on parameters that can be controlled in experiments, such as an external ionization rate, RF field amplitude, and background gas pressure, were investigated. © *2014 AIP Publishing LLC*.
[http://dx.doi.org/10.1063/1.4875379]

I. INTRODUCTION

There has been much progress over the last three decades in the development of microwave pulse compressors producing nanosecond output pulses of megawatt-to-gigawatt peak power with high (tens and hundreds) power gain. High-gain compressors are a promising alternative to high-power microwave sources driven by pulsed high-current relativistic electron beams as they employ well developed commercial magnetrons and klystrons operating at moderate voltages and being well proven for high repetition rates. A high gain is a feature of resonant compressors, in which an active element, a switch, is used to rapidly increase the coupling of a resonant cavity with a load for energy release, and the cavity Q-factor during the time of energy accumulation is much higher than that in the extraction phase.[1,2]

Presently, the microwave compressors with plasma switches based on gas discharge are mostly advanced. With these compressors, the power gains exceeding 20 dB are achieved in L-, S-, and X-bands; the peak output power level obtained in single-cavity S-band compressors reached 200–500 MW and with 2-stage compression, the peak power of 1.2 GW was obtained.[3] In X-band, compressors based on oversized Bragg resonators with plasma switches provided output pulses of up to 100 MW power with a gain of 11–12 dB.[4] A variety of plasma switch configurations have been developed including interference switches using high-pressure gas discharge in waveguide H-plane and Magic-tee junctions, switches using discharge tubes in the grooves of Bragg reflectors, switches based on fast transformation of different cavity eigenmodes, etc.

Nevertheless, despite experimental advances, processes occurring in plasma switches during microwave energy release from resonant cavities remain insufficiently understood. A particularly important point here is the quality of switching. An ideal switch in a high-gain compressor would fully open the cavity, so that an output pulse would have a rectangular waveform with a duration corresponding to the cavity double transit time and the output power would correspond to that of a traveling wave component in the cavity before switching. Meanwhile, in practice, the output power in high-gain compressors is reduced significantly. For instance, for the S-band compressor, in which probably the highest gain of 23 dB was achieved, a factor of 1.5 for the power reduction was reported.[5] In the X-band compressor of 20 dB gain, the output power was reduced by a factor of two.[6] Also, the waveforms of output pulses generated by compressors with plasma switches are rather far from rectangular. Evidently, the switching losses and waveform distortion are determined by the processes in the plasma discharge—ionization, excitation, scattering, and microwave energy dissipation in the plasma. The plasma represents a complicated medium—dispersive, dissipative, strongly non-stationary and non-linear, and a compressor output power changes in time according to the dynamics of the plasma electron density and electron-neutral collisions. To our knowledge, so far, neither theoretical studies nor numerical research concerning the problem of the influence of plasma discharge dynamics on the microwave compressor output pulse have been carried out.

In this work, the process of microwave energy release from a compressor is investigated numerically for a simple model representing a rectangular-waveguide-based cavity and H-plane tee as a switch filled with a gas at high pressure. Simulations allowing one to directly obtain the compressor output power versus time were carried out using the fully electromagnetic 3-D particle-in-cell (PIC) code MAGIC.[7] Different options for introducing the plasma provided by MAGIC were employed. These include PIC simulations with

either artificial or impact gas ionization, plasma representation as a conductive gas whose conductivity is determined by the electron mobility, and hybrid simulations combining macroparticles and gas conductivity model. In Sec. II, the main results of the performed simulations are presented.

II. SIMULATION RESULTS

All simulations were performed for the system geometry shown in Fig. 1. It consists of the waveguide sections having an identical standard cross-section (72 mm × 34 mm) and silver walls; these are input and output sections, a cavity section, and an H-plane tee with the shorted side arm. The input iris of 4 mm thickness has the circular coupling hole, 27 mm in diameter, filled with a dielectric of $\varepsilon = 2.25$. At the input port, the electromagnetic wave in the TE_{10} mode was injected into the system; the amplitude of the RF voltage across the waveguide in the center was set at 15 kV in all simulations. This corresponds to an input power of ≈225 kW at a resonant frequency of $f = 2.9802$ GHz.

The microwave energy storage (compressor charging) was simulated without introducing plasma; the electromagnetic fields obtained in this simulation were then used as preset fields to simulate the output pulse extraction with the appearance of plasma. The results of the simulation of the compressor charging are presented in Figs. 2 and 3. It is seen from Fig. 2 that there is almost no reflected wave in the input region, and leakage into the output region is negligibly small. It should also be noted that the E_z-field amplitude in the tee side arm is considerably higher than those in the cavity waveguide; one can see this when comparing the middle and bottom plots of Fig. 2. In Fig. 3, the growth of the RF voltage across the cavity waveguide in time is shown. It is seen that in the end of this simulation ($t \approx 1.1\ \mu$s), the RF voltage reaches the value of ≈220 kV. The ratio of half this value to the input RF voltage amplitude (15 kV) gives the cavity gain of ≈17.3 dB. This gain corresponds to ≈12.1 MW power of the traveling wave component of the cavity field—the figure to be compared to the compressor output power obtained in the simulations below.

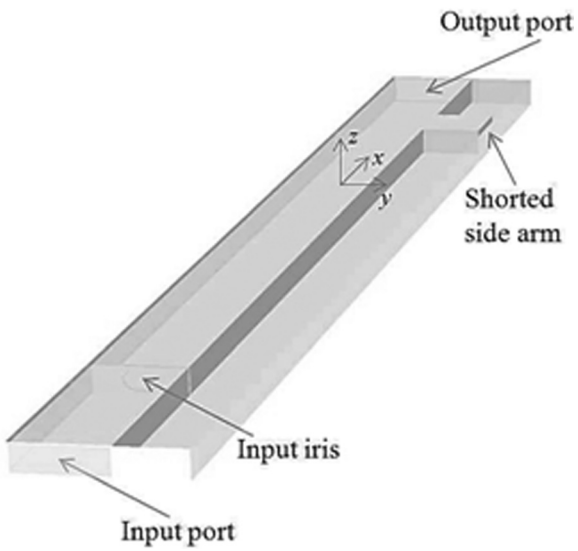

FIG. 1. 3-D view of the simulated compressor.

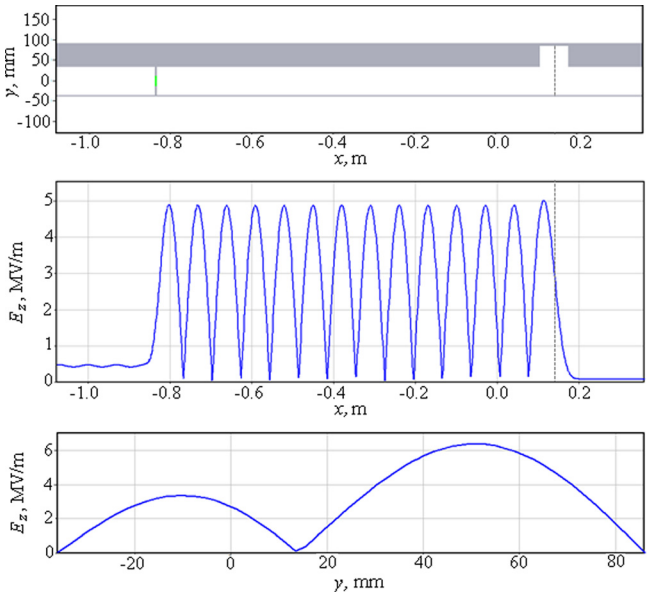

FIG. 2. Standing wave pattern at the compressor charging. Top: *x*-*y* plane of the simulation region. Middle: Profile of the E_z-field averaged over the oscillation period along the waveguide centerline ($y = z = 0$) at $t \approx 556$ ns from the beginning of the simulation. Bottom: same as middle along the line shown at the top as dashed line ($x = 14.4$ cm, also shown as dashed line at the middle).

A. Simulations with setting an artificial ionization

The microwave energy release from the compressor was simulated by introducing plasma in the region of maximal RF electric field in the tee side arm, at the quarter guide wavelength from the shorting plane (see Fig. 2, bottom). The simplest way to generate plasma is to use the available in the MAGIC code option of setting the rate of ionization, dn_e/dt (n_e is the electron density), i.e., electron-ion pair production, in a background gas as an arbitrary function of coordinates and time. The electrons, which are set in this way, interact with neutrals according to built-in interaction cross-sections. This influences, however, only on their motion (energy losses depending on the gas sort and pressure) and does not result in neutrals ionizing and does not lead to electron avalanche; that means the ionization is set artificially. The ions of the produced plasma are considered immobile during a rather short time of the output pulse extraction.

PIC simulations of this kind were performed with different ionization rates being constants within certain different time intervals. The background gas was nitrogen. The ionization region was the 8-mm thick layer across the tee side arm

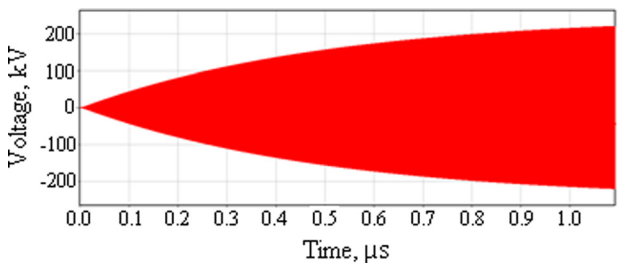

FIG. 3. Time dependence of the RF voltage across the cavity waveguide in the antinode of the standing wave pattern located in the middle of the cavity ($x = -37.78$ cm, $y = 0$).

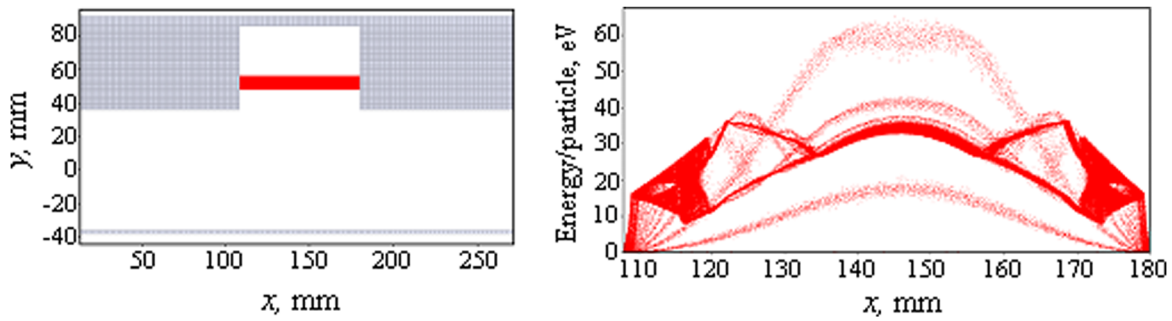

FIG. 4. Electrons in the tee side arm (left) and phase portrait in the *x-kinetic energy* plane (right) at 0.5 ns after the beginning of the ionization. The simulation used ionization rate $dn_e/dt = 5 \times 10^{20}\,\mathrm{cm^{-3}\,s^{-1}}$ at pressure $P = 10^5$ Pa.

as shown in Fig. 4. Also shown in Fig. 4 is an example of the electron phase space plot illustrating how electron energies are distributed along the wide wall of the waveguide. This plot was obtained at 0.5 ns from the start time of ionization, which is only about 1.5 period of the RF field, so that particles produced by the code at every time step acquire energy depending on the field phase in the moment of a particle appearance. As the plasma at atmospheric pressure is highly collisional, the electrons' energy is of the order of only tens of eV, in spite of a strong RF electric field ($\geq$80 kV/cm amplitude). There is, nevertheless, some correlation of electrons energies with the field profile over the waveguide wall. After the end of ionization, the electrons' phase space rapidly becomes uniform with maximal energy $\leq$20 eV.

The results of simulations showed that with the appearance of plasma, the standing wave pattern of RF fields is transformed into one of a traveling wave leaking out of the cavity. Depending on the density of the plasma determined by the ionization rate and time, only partial or almost complete reflection from the plasma layer takes place. The E_z-field at the plasma boundary decreases; it drops down to almost zero for almost complete reflection (see Fig. 5). In the case of partial reflection, when the wave reflected from the tee back into the cavity gets to the iris and is reflected back

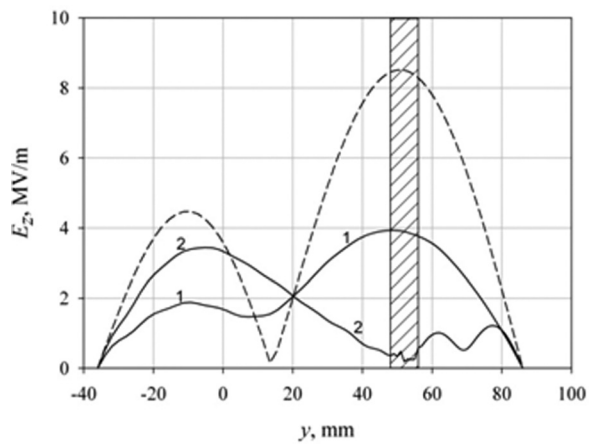

FIG. 5. Profile of the E_z-field averaged over the oscillation period along the centerline of the tee side arm waveguide (dashed line shown in Fig. 2) at 5 ns (dashed curve) and 8 ns (solid curves) after starting simulations. The ionization is turned on at 5.1 ns and off at 6.4 ns. The simulations used $P = 10^5$ Pa, $dn_e/dt = 1$–$5 \times 10^{20}\,\mathrm{cm^{-3}\,s^{-1}}$; 2–$5 \times 10^{21}\,\mathrm{cm^{-3}\,s^{-1}}$. The shaded area shows the ionization region.

again, a new standing wave pattern of smaller amplitude is formed. Accordingly, microwave energy is released toward the output port in portions of ever decreasing power. In Fig. 6, two different waveforms of the output pulse are shown. It is seen that in case of the lower density of the produced plasma (curve 1), the extracted power is less than half the stored power ($\sim$12 MW in the traveling wave component of the field built-up in the cavity), and there is a significant post-pulse power level. In the case of the longer ionization time leading to an order of magnitude higher plasma density (curve 2), the output power is almost the same as the stored one (just there is a considerably long rise-time of the pulse) and the post-pulse level is negligible.

Here, it should be noted that while qualitatively, the lower the E-field at the plasma boundary, the higher the output power is, right up to the stored one, the actual values of the plasma density, at which almost all, and even half the stored power is released seem to be too low for such efficient extraction. Indeed, in the simulation with ionization rate $5 \times 10^{20}\,\mathrm{cm^{-3}\,s^{-1}}$ and duration 1.3 ns, the plasma frequency of the produced plasma $\omega_p \approx 4.55 \times 10^{10}\,\mathrm{s^{-1}}$. This value is much lower than the frequency of electron-neutral collisions $\nu \geq 10^{12}\,\mathrm{s^{-1}}$ typical at atmospheric pressure and tens eV electron energies.[8] The circular frequency of microwave oscillations $\omega = 2\pi f < \omega_p \ll \nu$ as well. In these conditions, for the model of cold collisional plasma, the plasma permittivity $\varepsilon(\omega) \approx 1 - \omega_p^2/\nu^2 + i\omega_p^2/\omega\nu$,[8] and the electromagnetic wave reflection from the boundary of such a plasma is very small. Hence, one could expect an extracted microwave power to be much less than half the stored power, as in Fig. 6. The reason for this discrepancy is in the inaccuracy of calculations in the PIC simulations of the plasma whose Debye radius is significantly less than the computational grid cell size.[9] To avoid this, the grid cell size in simulations at $P = 10^5$ Pa and plasma densities of $\sim 10^{12}\,\mathrm{cm^{-3}}$ should be of the order of 0.1 mm or less. Simulations with ionization rate $5 \times 10^{20}\,\mathrm{cm^{-3}\,s^{-1}}$ and duration 1.3 ns were carried out for the cell size decreasing from 2 mm to 0.5 mm. The results of these simulations showed that the output power decreases considerably and with a finer grid, a decrease is larger. Nevertheless, even the smallest cell size of 0.5 mm remains insufficiently small as it still resulted in too a high percentage, $\approx$34%, of the power extraction. Further reducing the cell size would lead to an impractical time for simulations to run. Thus, PIC simulations with artificially produced plasma

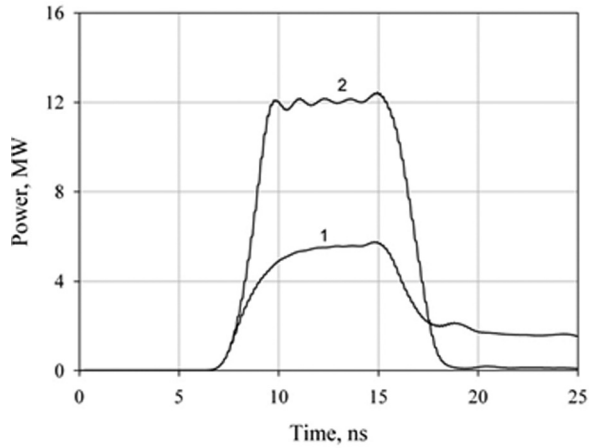

FIG. 6. Output power (Poynting flux at the output port averaged over the oscillation period) vs. time. Simulations used $dn_e/dt = 5 \times 10^{20}\,\mathrm{cm^{-3}s^{-1}}$, $P = 10^5$ Pa. The ionization is turned on at 5.1 ns. The duration of the ionization is: 1–1.3 ns; 2–13 ns.

only qualitatively describe the process of microwave energy release from high-power, high-gain compressors operating at atmospheric pressures; they are not appropriate for adequate quantitative evaluation of the output power, at least with the present capabilities of personal computer hardware.

B. Simulations using gas conductivity model

The MAGIC code contains another model that is more suitable to simulate dense plasma. This is the gas conductivity model, in which plasma is represented by a conductive gas filling the simulation space.[7,10] This model is based on the concept of mobility, i.e., the gas conductivity is determined by the electron and ion density and mobility depending on the electric field, pressure, and temperature $\sigma_{gas} = e(\mu_e n_e + \mu_p n_p + \mu_n n_n)$. Here, μ and n are the mobilities and densities and indices e, p, n correspond to electrons, positive, and negative ions, respectively. The densities evolve according to the equations accounting for the electron avalanche, electron-neutral attachment, electron-ion recombination, and positive-negative ion neutralization

$$\frac{dn_e}{dt} = Q_e + (\alpha - \beta)n_e - \alpha_e n_e n_p,$$
$$\frac{dn_n}{dt} = \beta n_e - \alpha_i n_n n_p,$$
$$n_p = n_e + n_n.$$

The source term Q_e can be set as a function of coordinates and time; such a simulation would not include any particles. Otherwise, Q_e is calculated using ionization cross-sections for primary electrons treated by the PIC algorithm; this would be a hybrid model. The coefficients α (avalanche), β (attachment), α_e (recombination), and α_i (neutralization) are field- and pressure-dependent, as well as are the mobilities, so that simulations using the gas conductivity model can be considered, in some sense, self-consistent. In all simulations below, for coefficients' dependences on the field, pressure, and temperature, the models provided by the MAGIC for air were applied.

Important simulations that can be performed using the gas conductivity model are simulations with zero Q_e and non-zero initial electron density. In this manner, simulation of compressor charging accounts for the presence of natural electron background, and thus the level, up to which the RF field can be accumulated in the cavity before the self-breakdown at a given pressure, is determined. Such simulations were performed with the initial electron density corresponding to the cosmic background, $n_e|_{t=0} = 10^4\,\mathrm{cm^{-3}}$, within the tee side arm. Typical results are presented in Fig. 7. One can see that the electron density begins to grow in accordance with the standing wave pattern of the E-field in the cavity (top left). The density in the point of maximal field reaches the maximal value as high as $\approx 1.76 \times 10^{13}\,\mathrm{cm^{-3}}$ (bottom left), which is an order of magnitude higher than the plasma density set in PIC simulations with artificial ionization. The density growth

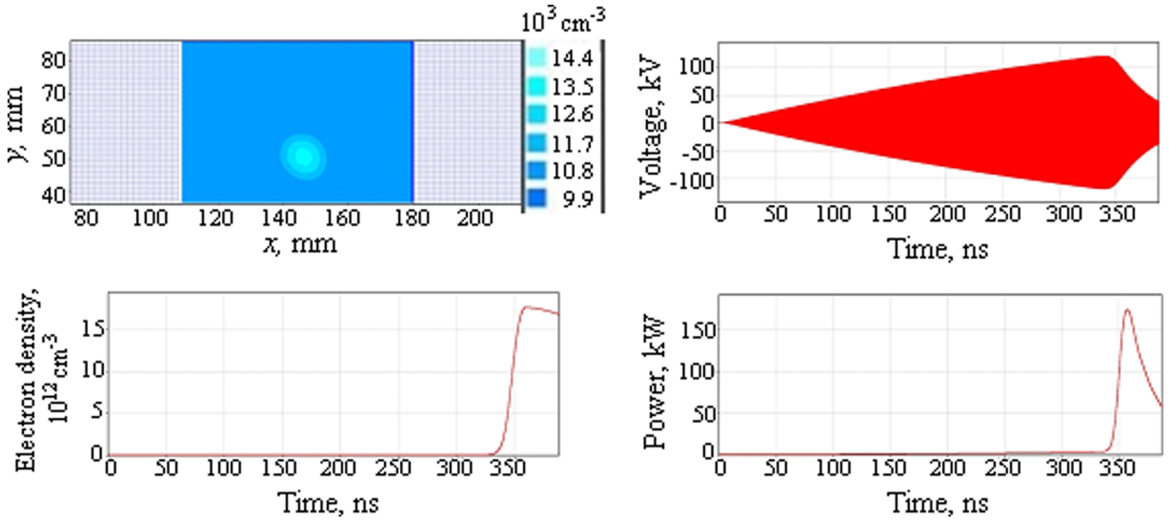

FIG. 7. Compressor charging up to self-breakdown at $P = 10^5$ Pa. Top left: contour plot for the electron density (plane $z = 0$ within the tee side arm) at an early stage of charging (200 ns since the beginning). Bottom left: electron density vs. time in the point of maximal RF electric field. Top right: RF voltage in the middle of the cavity (as in Fig. 3) vs. time. Bottom right: RF power at the output port vs. time.

(avalanche development) stops the field build-up at $t \approx 340$ ns (top right) and accordingly, the RF signal appears at the output (bottom right). Let us note that the maximal RF voltage in the cavity corresponds to ≈3.6 MW stored power, while the peak output power is only of ≈174 kW, even less than the input power. This is a typical situation of self-breakdown, which occurs rather frequently in experiments.

In order to get a valuable output signal, one needs to trigger the plasma discharge externally, i.e., to turn on the source term Q_e in a simulation before the microwave energy storage would stop. The efficiency of the output power extraction will then depend on the external ionization rate and duration, and, of course, on the gas pressure. In addition, the output power is also determined by the stored power, which strongly depends on the pressure since the E-field before the gas self-breakdown gets higher with increasing pressure. To investigate these dependences, simulations at different pressures were performed: first, from simulations with zero Q_e, a certain time moment when the electron density reaches the order of 10^{10} cm^{-3} was determined and then simulations with different Q_e turned on at this moment were run. The source term was set within the 8-mm thick layer across the tee side arm (same as the ionization region in Subsection II A).

In Fig. 8, the results of these simulations are presented for the constant $Q_e = 10^{22}$ cm^{-3} s^{-1} operating for only 5 ns; the output pulses are shown starting from the moment of the beginning of external ionization. It should be noted that the electron density rises up to values, which are a bit less than 5×10^{13} cm^{-3} that would be produced by the source term only ($n_e \approx 4.6 \times 10^{13}$ cm^{-3} for $P = 10^5$ Pa and 4.3×10^{13} cm^{-3} for $P = 3 \times 10^5$ Pa), and as the external ionization ends, the density begins to decrease due to recombination and attachment processes. The output power decreases accordingly; the moment of time corresponding to maximums in the output pulses is shifted with respect to the end of ionization by the time needed for the leaking wave to get to the output port. For the lower pressures, nevertheless, the output pulses look quasi-rectangular (curves 1 and 2) due to the lower rates of the electron density decrease. In addition, with increasing pressure, the efficiency of power extraction decreases significantly because of Joule losses, as seen from the right plot of Fig. 8. On the other hand, a higher pressure allows for a longer duration of energy accumulation, so that the source term is turned on at a higher stored power; therefore, the output power itself increases with increasing pressure up to some maximum value. This is clearly seen from the left plot of Fig. 8—the power obtained at $P = 3 \times 10^5$ Pa is only very slightly higher than that obtained for $P = 2.5 \times 10^5$ Pa, which, in turn, is much higher than in the case of lower pressures.

The optimal pressure, at which the output power is maximized for a given input power is an important characteristic of the system in practice. Naturally, the optimal pressure depends on the maximal electron density produced as a result of external ionization. If the density is sufficiently high, it is the minimal pressure at which the process of RF field build-up saturates without self-breakdown; this is $P \sim 3 \times 10^5$ Pa for our simulations with ≈225 kW input power. For lower densities, the optimal pressure is lower. In Fig. 9, the same results as shown in Fig. 8 are presented for the source term of 3×10^{21} cm^{-3} s^{-1} turned on for 10 ns. It is seen that the highest output power is achieved at $P = 2.5 \times 10^5$ Pa (curve 3 in the left plot). In addition, Fig. 9 illustrates decreasing efficiency of power extraction at a lower electron density produced by the source term. Comparison of the peak output power values in Figs. 8 and 9 shows that the efficiency decreases by ~12% for $P = 10^5$ Pa and by a factor of ~1.7 for $P = 3 \times 10^5$ Pa. Finally, one can see that all output pulses in Fig. 9 have rather triangular waveforms, which are caused by longer rise-times in the electron density.

Thus, simulations using the gas conductivity model give reasonable results and allow one to investigate the dependences of the compressor output on parameters that can be really controlled, particularly, to find an optimal pressure maximizing output power. A disadvantage of the model not including particles in the simulations is in the fact that the plasma density changes in time locally. Meanwhile, the diffusion of electrons definitely influences the ionization process and, hence, the output pulse power and waveform; it can be taken into account using a hybrid model.

C. Hybrid simulations

In hybrid modelling, both macroparticles and conductive gas are present in the simulations. Macroparticles contribute to the gas ionization via the source term in the gas conductivity model, which is calculated from PIC dynamics and ionization cross-sections, namely, $Q_e = \frac{qN}{e\Delta V} \sum_i v_i \sigma_{ion}(v_i)$, where q and v_i are the charge and velocity of a macroparticle, respectively, σ_{ion} is the cross-section, N is the neutral gas number density, and ΔV is the cell volume of the

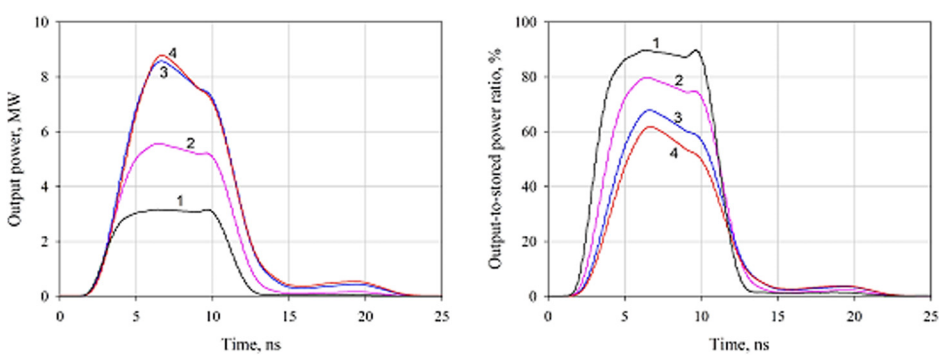

FIG. 8. Output power (left) and efficiency of power extraction (right) obtained from the simulations with external ionization rate $Q_e = 10^{22}$ cm^{-3} s^{-1} set from $t = 0$ until $t = 5$ ns at different pressures: $P = 1-10^5$ Pa; 2–1.7×10^5 Pa; 3–2.5×10^5 Pa; 4–3×10^5 Pa.

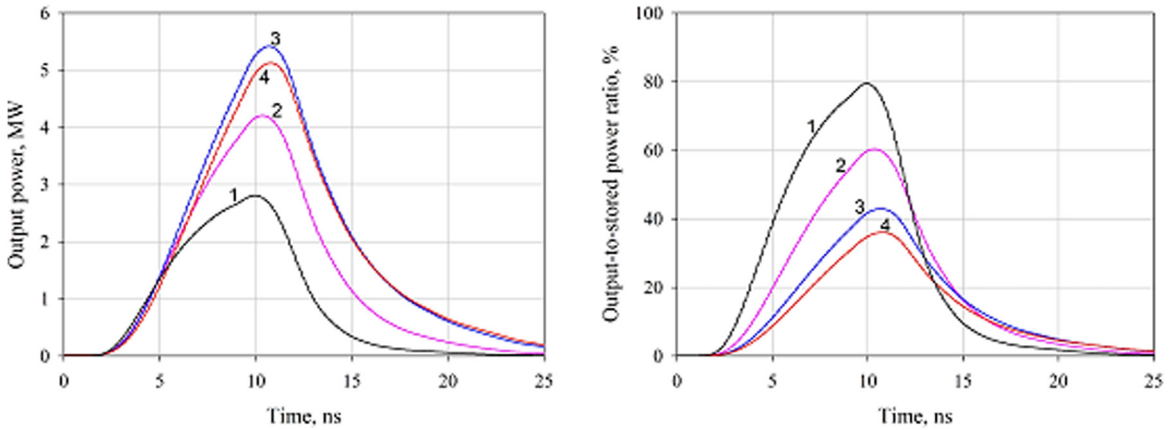

FIG. 9. Same as Fig. 8 except for ionization rate $Q_e = 3 \times 10^{21}$ cm^{-3} s^{-1} and duration of 10 ns.

computational grid. In addition, particles may produce electron-ion pairs via the impact model of ionization available in MAGIC; the generated electrons participate in the ionization of neutrals as well.

Hybrid simulations were performed for the case when at the beginning of simulation there are primary electrons in the tee side arm populating the volume of cubic form ($8 \times 8 \times 8$ mm^3) around the antinode of the RF electric field in the center of the waveguide cross-section (see Fig. 10). Preset RF fields correspond to the stored power of $\approx$12.1 MW ($\geq$80 kV/cm field amplitude in the populated volume), as in Subsection II A. Accordingly, due to the interaction with neutrals, the energy of electrons becomes $\sim$20 eV, as seen in Fig. 10.

Results of the simulation, in which no generation of electron-ion pairs by the primary electrons was included (i.e., MAGIC command for impact ionization was not used), are presented in Figs. 11 and 12. In Fig. 11, one can see the electron density calculated by the gas conductivity model in the center of the volume populated with the primary electrons and the output power as a function of time. The electron density rises up to $\sim 1.25 \times 10^{14}$ cm^{-3} in about 2.5 ns; then, it saturates and begins to slightly decrease. Meanwhile, the output power continues to rise until about 11 ns. Evidently, this long-lasting increase in the output power is connected with the diffusion of the primary electrons leading to ionization outside the initially populated region. As a result, the plasma (conductive gas) volume expands, the reflection from it increases with time, and the output power increases accordingly. Particle diffusion and plasma expansion are illustrated in Fig. 12; it is seen that the plasma region expands mostly along the direction of the electric field.

One can compare the output pulse waveform obtained in the hybrid simulation with that of the purely "gas conductivity" simulation without particles in which diffusion is not accounted for. For such simulation, the constant source term $Q_e = 10^{23}$ cm^{-3} s^{-1} was set within the same cubic volume as where the primary electrons were seeded in the hybrid simulation. The value of Q_e was taken to be about the highest rate of electron density rise that appears in the hybrid simulation and can be estimated from the left plot of Fig. 11. The results are presented in Fig. 13. It is seen that the rise in the output power correlates with the electron density rise; after the density saturates, a "flat-top" part follows in the output pulse waveform. The density at saturation in Fig. 13 is higher than that shown in Fig. 11. The peak power, however, is significantly higher for the hybrid simulation owing to the plasma expansion as a result of electron diffusion. It should be noted that the peak output power of $\sim$4.4 MW obtained in the hybrid simulation is rather low compared to the stored power. This is related to the dimensions of the plasma, which, even at the end of the simulation, occupies only a small part of the waveguide cross-section (see bottom plots of Fig. 12). Naturally, the efficiency of power extraction from the cavity is lower than that shown in Figs. 8 and 9 since in those simulations the source term was set within the entire waveguide cross-section.

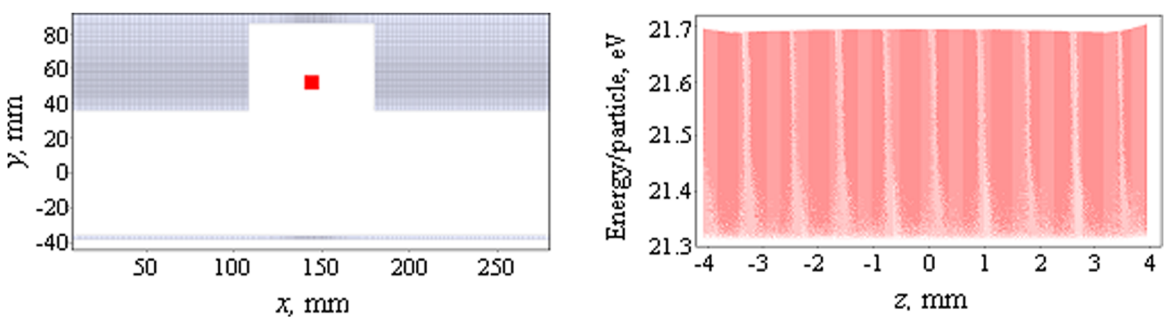

FIG. 10. Electrons in the tee side arm (left) and phase portrait (kinetic energy vs. z, right) at 0.3 ns after the beginning of the hybrid simulation. The gas is nitrogen, $P = 10^5$ Pa, initial charge density is 10^{-11} C/cm^3; initial velocities are randomly distributed from 0 to 10^8 cm/s.

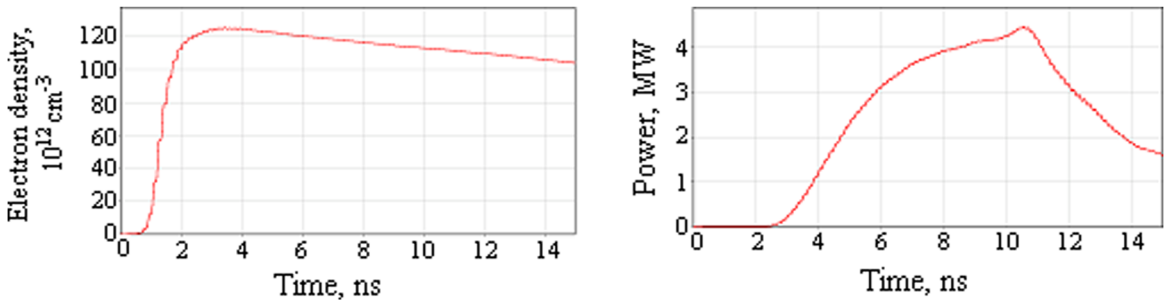

FIG. 11. Hybrid simulation with primary particles only; parameters are as in Fig. 10. Left: electron density evolved according to the gas conductivity model in the point of maximal preset RF electric field vs. time. Right: RF power at the output port vs. time.

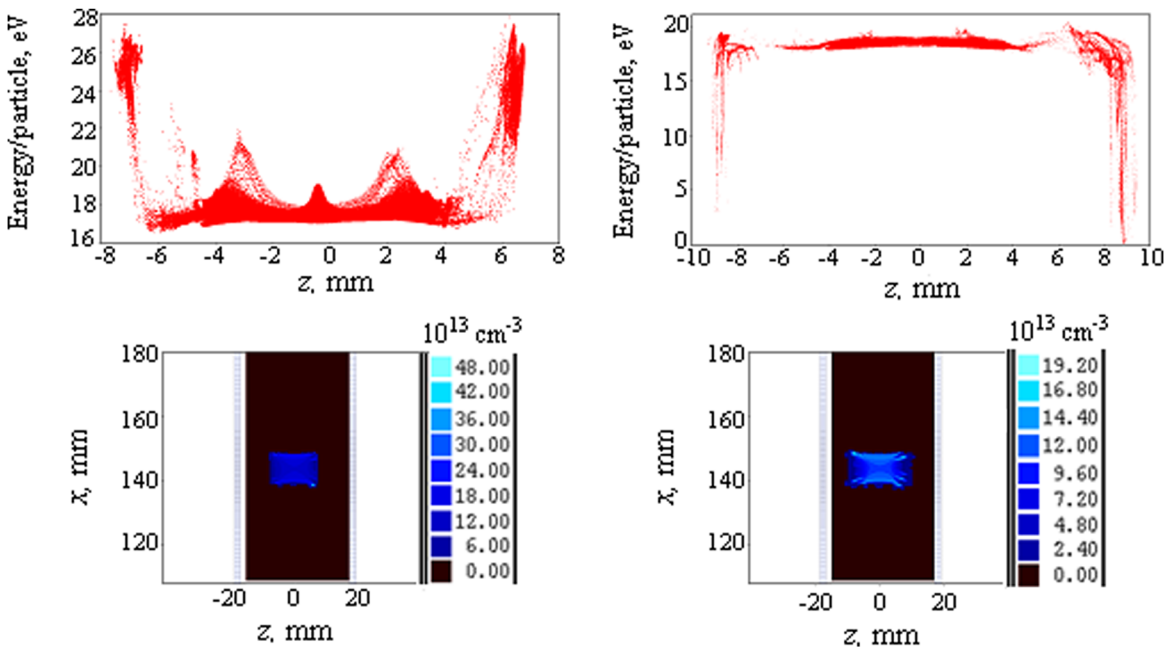

FIG. 12. Same simulation as in Fig. 11. Top: particles' phase portraits (kinetic energy vs. z-coordinate) at $t = 7.5$ ns (left) and 14.5 ns (right). Bottom: contour plots for the electron density within the tee side arm waveguide cross-section (z-x plane) at the middle of the initially populated volume. $t = 7.5$ ns (left) and 15 ns (right).

The hybrid simulations using the gas conductivity model in association with impact ionization were also carried out. In these simulations, the MAGIC option of electron-ion pairs' indirect creation[7] was used, so that other charged particles were generated in addition to the primary electrons. The equations of the gas conductivity model then include a leakage term accounting for this charge transfer from the conductive gas to particles. The results of these simulations, however, exhibit too strong, seemingly inappropriate electron diffusion and avalanche. As shown in Fig. 14 (top left plot), the output power in such simulation turns out to be comparable with the stored power, and the output pulse duration is shortened with respect to the cavity double transit time. It is seen that the electron density evolved according to the gas conductivity model (top right plot) becomes 1–2 orders of magnitude higher than in the simulation with the primary

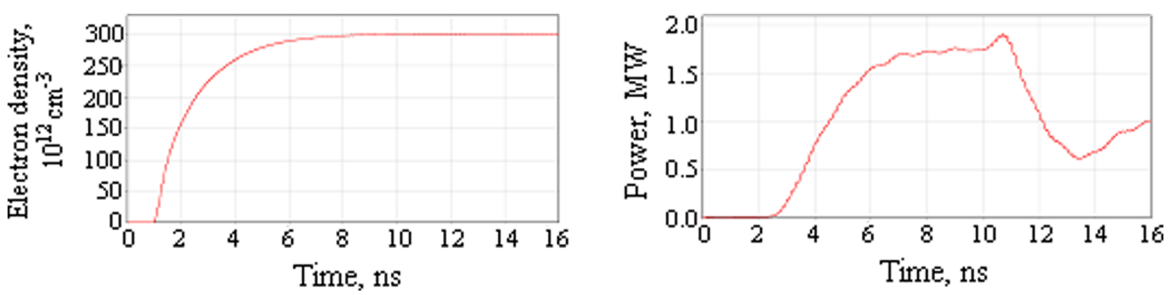

FIG. 13. Same as in Fig. 11 for the simulation without particles. The source term $Q_e = 10^{23}$ cm^{-3} s^{-1} is set within the same volume as shown in Fig. 10 and is turned on at $t = 1$ ns.

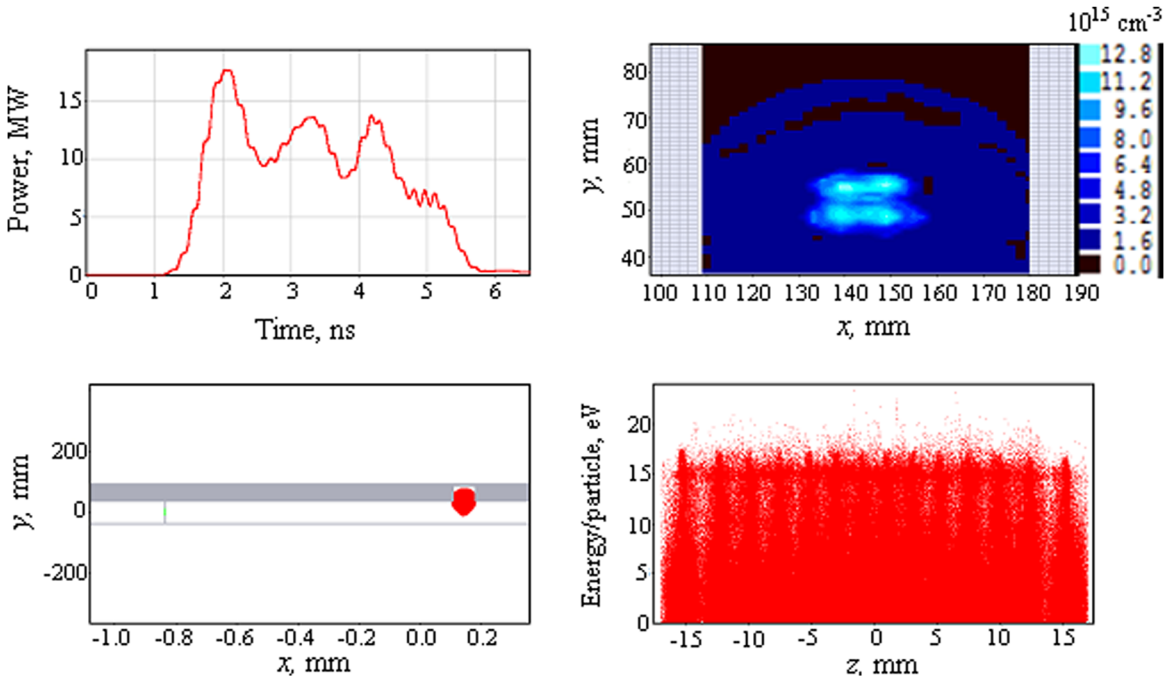

FIG. 14. Hybrid simulation with primary particles generating electron-ion pairs; parameters are as in Fig. 10. Top left: output power vs. time. Top right: contour plot for the electron density calculated from the gas conductivity model within the tee side arm (x-y plane at $z = 0$); $t = 4$ ns. Bottom: particles in x-y plane (left) and kinetic energy vs. z-coordinate (right) at $t = 4.5$ ns.

particles only. The reason for that is in an excessive, in spite of limiting imposed by MAGIC, generation of particles. As a result, in the simulations, plasma rapidly occupies almost all the volume of the tee side arm and penetrates into the cavity waveguide region (bottom plots), thus terminating the output pulse. To the best of our knowledge, there is no experimental evidence for such pulse shortening in high-power compressors, so this result seems rather inadequate.

The hybrid simulations combining ionization via particle generation and gas conductivity model were performed not only for the case of primary electrons populating the volume shown in Fig. 10 but also for electron beam injection into the tee side arm at a quarter wavelength distance from the shorting plane through the narrow or wide wall of the waveguide. All results exhibited similarly excessive diffusion in all directions. Nevertheless, despite these unsatisfactory results, one can consider such combined hybrid modeling as an approach that is potentially more correct than hybrid simulations with primary particles only. Evidently, proper limitations on the generation of particles should be found in order to obtain adequate results.

III. CONCLUSIONS

With the use of the MAGIC code, numerical simulations of the microwave energy release from a high-gain pulse compressor with a switch based on a high-pressure plasma discharge have been performed. Purely PIC simulations were found to be inappropriate for studying the dynamics of plasma formation in the switch in connection with the extraction of the microwave pulse. Simulations using the gas conductivity model contained in the MAGIC code and hybrid simulations combining the plasma representation as a conductive gas with particles treated by the PIC algorithm allowed for investigating the dependences of the compressor output pulse peak power and waveform on parameters that can be controlled in experiments.

The effect of self-breakdown with a minor output has been demonstrated in simulations of the compressor charging with an initial background electron density. It was shown that for a given input power and external ionization rate, there is an optimal pressure maximizing output power; the efficiency of power extraction, however, decreases with increasing pressure. The rise of the output power in time correlates with the rise of the plasma density; in addition, the output power rises with the expansion of the volume occupied by the plasma as a result of electron diffusion. Thus, to increase the efficiency of power extraction from the cavity and shorten the rise time of the compressor output pulse, one needs a higher rate of ionization when the discharge is triggered and/or faster expansion of the plasma volume.

It is important to perform simulations of the output pulse extraction with adequate, self-consistent models for setting external ionization rate, which are to be developed for different methods of discharge triggering such as laser triggering, spark triggering, etc. Such simulations, as well as hybrid simulations, correctly combining ionization by particles production with the gas conductivity model are planned for our future work.

ACKNOWLEDGMENTS

The work was partially supported by the BSF Grant No. 1009212.

[1]J. Benford, J. A. Swegle, and E. Schamiloglu, *High Power Microwaves*, 2nd ed. (Taylor & Francis, New York, 2007).

[2]A. N. Didenko and Yu. G. Yushkov, *Powerful Microwave Pulses of Nanosecond Duration* (EnergoAtomizdat, Moscow, 1984) (in Russian).
[3]S. Novikov, Yu. Yushkov, S. Artemenko *et al*., "Development of high-power microwave compressors," in *Proceedings of 16th IEEE Pulsed Power Conference (PPPS-2007), Albuquerque, NM, 17–22 June 2007*, Vol. 2, pp. 1822–1825.
[4]A. L. Vikharev, A. M. Gorbachev, O. A. Ivanov *et al*., "Two-channel 100-MW microwave compressor for the three-centimeter wavelength range," Radiophys. Quantum Electron. **51**(8), 597–609 (2008).
[5]S. N. Artemenko, V. A. Avgustinovich, and S. A. Novikov, "Single-mode interference switches of high power resonant microwave compressors," in *Proceedings on 14th Symposium on High-Current Electronics, Tomsk, Russia, 10–15 September 2006*, pp. 410–412.
[6]S. N. Artemenko, V. A. Avgustinovich, V. L. Kaminskii *et al*., "Experimental investigation of a 25-MW microwave (3-cm range) compressor prototype," Tech. Phys. **45**(12), 1608–1611 (2000).
[7]B. Goplen, L. Ludeking, D. Smithe, and G. Warren, "User configurable MAGIC code for electromagnetic PIC calculations," Comput. Phys. Commun. **87**(1/2), 54–86 (1995).
[8]Yu. P. Raizer, *Gas Discharge Physics* (Springer-Verlag, Berlin, 1991).
[9]C. K. Birdsall and A. B. Langdon, *Plasma Physics via Computer Simulation*, The Adam Hilger Series on Plasma Physics (IOP Publishing, 1991).
[10]A. J. Woods and L. D. Ludeking, "MAGIC electromagnetic FDTD-PIC code dense plasma model comparison with LSP," Open Plasma Phys. J. **3**, 73 (2010).